ISSN 1075-7015, Geology of Ore Deposits, 2022, Vol. 64, No. 5, pp. 281–291. © Pleiades Publishing, Ltd., 2022.
Russian Text © The Author(s), 2022, published in Geologiya Rudnykh Mestorozhdenii, 2022, Vol. 64, No. 5, pp. 451–461.

Invisible Gold and Other Impurity Elements in Pyrite and Arsenopyrite of Disseminated Ores of the Kyuchus Deposit (Sakha Republic (Yakutia))

N. V. Sidorova[a], *, A. V. Volkov[a], **, E. V. Kovalchuk[a], E. A. Minervina[a], and L. A. Levitskaya[a]

[a] *Institute of Geology of Ore Deposits, Petrography, Mineralogy, and Geochemistry, Russian Academy of Sciences, Moscow, 119017 Russia*

**e-mail: nsidorova989@mail.ru*

***e-mail: tma2105@mail.ru*

Received June 23, 2021; revised November 16, 2021; accepted November 18, 2021

Abstract—For the first time, EPMA and LA-ICP-MS data were obtained for the Kyuchus Au–As–Sb–Hg deposit on variations in the grades and zonal distribution of gold and other impurity elements in gold-bearing sulfides of disseminated ores. Two types of zoning have been found in pyrite: (1) zoning with the central zone depleted in impurities bearing As (1.5–1.9 wt %) and Au (~up to 5 ppm), an impurity-enriched intermediate zone (As up to 5.4 wt %), and an outer rim with contents of As of about 3 wt % and Au (LA-ICP-MS 20–30 ppm; EPMA 0.03 wt %); (2) zoning with central zones enriched in arsenic (up to 7 wt %) and markedly arsenic-depleted (3.6–5.8 wt %) rims with Au content up to 310 ppm (EPMA). Arsenopyrite also has a zoned structure with a central zone enriched in Sb; the amount of As and Au increases towards the edges of crystals. Compared to pyrite, arsenopyrite is characterized by higher Co, Ni, Ag, Sb, Au, Hg contents and lower Cu contents. According to the EPMA data, the Au content in arsenopyrite reaches 0.2 wt %; in pyrite, 0.03 wt %. In arsenopyrite, the maximum gold concentrations are confined to the edges of the crystals. In pyrite, the maximum Au concentrations are in marginal rims and cribrose-cellular regions of grains. For both sulfides, no significant correlation was found between gold or other elements.

Keywords: Northern Yakutia, Kyuchus deposit, pyrite, arsenopyrite, invisible gold, EPMA, LA-ICP-MS

DOI: 10.1134/S1075701522040067

INTRODUCTION

The problem of invisible gold in deposits is of great scientific and practical importance (Cabri et al., 1989; Cathelineau et al., 1989; Chryssoulis and Cabri, 1990; Genkin et al., 1998). The study of the nature and forms of finding gold makes it possible to reveal the formation conditions of ores and to create the scientific principles for their processing technology. For gold–antimony (mercury–tungsten–antimony) deposits with gold–sulfide disseminated ores in carbonaceous–terrigenous strata (Olimpiadninskoe, Veduga (Yenisei Ridge), Mayskoe (Chukotka), Sarylakh, Sentachan (Yakutia), Suzdalskoe, (Kazakhstan) etc.) is characterized by fine gold in pyrite and arsenopyrite, which makes up a significant part of the total ore balance (Volkov and Sidorov, 2017). The main concentrator of so-called invisible (not determined by modern optical and electron microscopy methods) gold in these deposits is arsenopyrite, often with an acicular habit (Genkin et al., 1994; Volkov et al., 2007; Kovalev et al., 2012). At large gold–antimony deposits in terrigenous sediments of the Adycha–Taryn zone of the Sarylakh and Sentachan deposits, gold concentrations in pyrite reach 236 and 470 ppm, respectively, and in arsenopyrite, 495 and 1000 ppm (Genkin et al., 1998; Bortnikov et al., 2010). A chemically bound form of gold was identified by X-ray absorption spectroscopy (XANES) in arsenopyrite from the Sentachan deposit (Cabri et al., 2000). The Kyuchus deposit, which is of the gold–sulfide disseminated type, is localized in the Yana fault zone (northern extension of the Adycha–Taryn zone) in Triassic terrigenous strata (Novozhilov and Gavrilov, 1999). Earlier, the gold content of pyrite and arsenopyrite of the Kyuchus deposit was estimated by neutron activation analysis (Berzon et al., 1999); chemical and ion-plasma etching with further study of the surfaces of sulfides by STM revealed the position of fine gold particles in sulfides (Moskvitina et al., 2019). This paper presents the results of EPMA and LA-ICP-MS studies of pyrite and arsenopyrite from disseminated and banded sulfide ores without visible gold at the Kyuchus deposit.

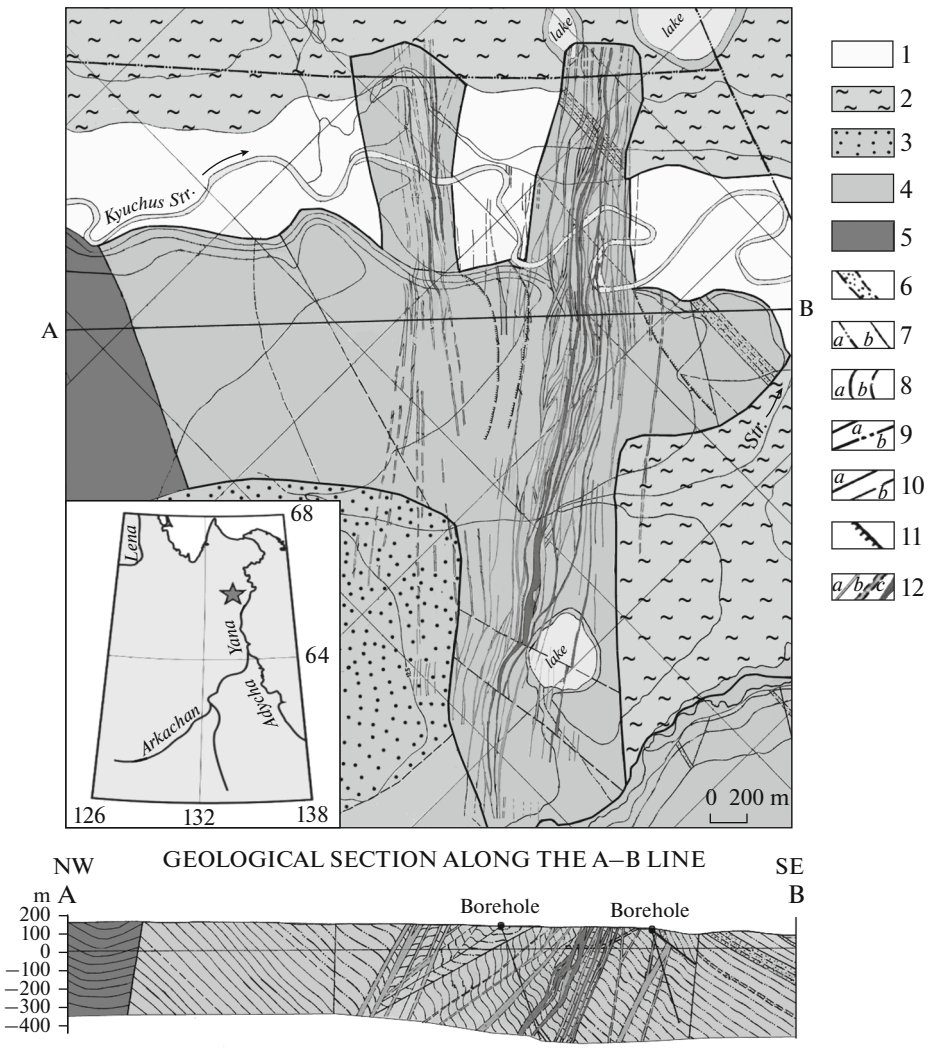

Fig. 1. Geological map of Kyuchus deposit (based on materials of Yana GRE with simplifications). Inset shows geographic location of deposit. (1–3) Quaternary deposits: (1) alluvial pebbles, sandy loam, loam; (2) Zyryan–Karga horizon: alluvial pebbles, sandy loam, loam; 3, polygenic alluvial–deluvial and solifluction deposits; (4, 5) Middle Triassic: (4) Ladinian stage, intercalation of calcareous siltstones with sandstone beds; (5) Anisian Stage: calcareous siltstones and mudstones with rare sandstone beds; (6) horizons of sandstones; (7) structural lines (only in the section): (*a*) silty sandstone sequences, (*b*) siltstone sequences; (8) boundaries between noncoeval rocks: (*a*) reliable, (*b*) inferred; (9) main faults: (*a*) confirmed, (*b*) inferred; (10) secondary faults: (*a*) confirmed (*b*) inferred; (11) thrusts; (12) mineralized zones (*a*), orebodies (*b*, *c*): (*b*) inferred, (*c*) confirmed.

GEOLOGICAL STRUCTURE AND MINERAL COMPOSITION OF KYUCHUS ORES

The Kyuchus deposit is located in the north of the Verkhoyansk district in the Sakha Republic (Yakutia) beyond the Arctic Circle, in the lower reaches of the Kyuchus River, a left tributary of the Yana River (Fig. 1, inset). The deposit was discovered in 1963 by the Central Search and Survey Expedition of the Yakut Territorial Geological Administration during a state geological survey at a scale of 1 : 200000. The Kyuchus deposit is one of the largest gold deposit of the Sakha Republic (Yakutia). The reserves of the deposit in the sum of categories ($C_1 + C_2$) are 175.2 t; the predicted resources ($P_1 + P_2$) are 51.1 t.

Geology

The deposit is located in the Verkhoyansk–Chukotka fold region on the southeastern flank of the Kular fold-block uplift in the junction zone with the Polusnensky synclinorium within the deep-seated Yana fault (Berzon et al., 1999). The ore field is located in an intense linear fold zone and is composed of 1400 m thick terrigenous formations of the Middle Triassic Ladin Stage, which make up the middle part of the Verkhoyansk Terrigenous Complex (Fig. 1). The lower Upper Permian–Middle Triassic part of the complex, 4–6 km thick, outcrops to the west in the core of the Kular anticlinorium. The upper, Upper Triassic–Lower Cretaceous part of the complex, 8–10 km thick, outcrops to the east in the Poloustnoe synclino-

rium. The deposits of the Verkhoyansk Complex unconformably overlie Lower Paleozoic and Devonian–Lower Permian carbonate–evaporite sequences, the thickness of which is estimated at 3–4 km (Berzon et al., 1999). The lithological composition of the section is extremely noncontrasting (siltstones, mudstones, sandstones). The host rocks have a monoclinal eastern dip. An important geological and structural feature of the deposit is the absence of igneous rocks.

The Kyuchus ore field is a diamond-shaped block of flyschoid terrigenous rocks 6 × 6 km in size, bounded by two NE-trending transform fault sutures and two NW-oriented shear zones (Fig. 1). Sedimentary rocks within the deposit are bent into a submeridional anticline fold (Konyshev, 1995).

The ore field has a complex block-keyboard structure. It is densely mottled with sublatitudinal, submeridional, NE, and NW lower-order faults, rather faults that bound the field (Fig. 1). The ore-bearing zones dip to the northwest at angles of 55°–75° and pass from east to southwest for 2.2 km from the eastern limb of the anticline to its hinged part, then to the western limb. The orebodies are localized in NE fault structures oriented at angles of 35°–55° to the strike of the rocks. The pinching out of ore mineralization on the NE flank is due to the steep (more than 70°) bedding of rocks of the eastern flank of the anticline. In the central hinged part of the anticline, where the rocks are flattened to angles of 15°–60°, mineralized zones bear concentrated ores (Konyshev, 1995).

The orebodies of the Kyuchus deposit are crush, brecciation, and shear zones interspersed with gold–arsenic mineralization. A total of 13 orebodies have been explored, of which orebody no. 1 accounts for 70% of the reserves. The dimensions of the main orebodies are: extent of strike, 300–3500 m; extent of dip, 150–160 m (not contoured at depth); thickness, 1.1–4.5 m; steep dip (70°–80°); the expected depth of ore development from the surface is 1000 m or more (Fig. 1). The content of the main component is (on average) gold, 8.5 ppm. Associated components are silver, 1.5 ppm; arsenic, 1.7%; antimony, 0.5%; mercury, 0.024%.

Ore Textures

Disseminated, banded and vein types of ores are characteristic. Disseminated ores are represented by brecciated thinly layered siltstones and sandstones bearing sulfide, predominantly arsenopyrite–pyrite disseminations. The banded texture of the ore is due to the uneven layer-by-layer and interlayer concentration of sulfides. It is important to note that the sandstone interlayers contain denser sulfide disseminations than do the siltstone layers. Interlayers of carbonaceous mudstones are most often completely barren. In them, in contrast to the primary porous silty sandstones, the processes of metasomatic silicification and carbonatization, which accompanied the formation of disseminated ores, are weakly manifested.

Vein ores are represented by lenticular carbonate–quartz veins, lenses and veinlets; they occur in the central parts of crush zones (core veins), in contouring, diagonal, and multidirectional interboudin sutures of ore-bearing tectonic zones.

Ore Mineralogy

The major ore minerals in the deposit are arsenopyrite, pyrite, antimonite, native gold, cinnabar, and realgar; secondary ores are fahlores, metacinnobarite, sphalerite, orpiment, and chalcopyrite; rare ores are pyrrhotite, marcasite, chalcostibite, native mercury, and berthierite. There are four main, successively formed mineral assemblages at the deposit (Berzon et al., 1999): (1) pyrite–arsenopyrite; (2) antimonite–quartz; (3) cinnabar–metacinnabarite–kaolinite, and (4) carbonate (postproduction). The first three associations are gold-bearing, while the first is characterized by finely dispersed gold, in other cases—visible native gold.

Ores of Kyuchus belong to the type of "hard-to-enrich" and technologically "refractory" (Berzon et al., 1999). This is due to the presence of arsenic, organic carbon, mercury, and submicroscopic dissemination of the ground mass of gold in iron sulfides and sulfoarsenides, which, in turn, are finely dispersed in the host rocks (≤0.1 mm). The upper part of the orebodies to a depth of 40–80 m is represented by oxidized ores, while the lower part, by mixed and primary ores. Basic gold is associated with arsenopyrite, 40–1000 ppm; with pyrite, about 40 ppm; and with stibnite, 20–25 ppm; it is also associated with realgar and orpiment, up to 2 ppm. The upper parts of orebodies are enriched in cinnabar.

RESEARCH METHODS

Polished sections of pyrite–arsenopyrite ores were studied earlier in the reflected light of an optical microscope. Next, the polished surfaces of sulfides were scanned in backscattered (BSE) and secondary (SE) electrons using a scanning electron microscope (JSM-5610LV, Japan) with an energy dispersive attachment (INCA-Energy 450, Great Britain). The qualitative composition of micron-sized mineral segregations was obtained by SEM-EDS at IGEM RAS (analyst L.A. Levitskaya).

The chemical composition of the studied sulfides was obtained on a JXA-8200 X-ray spectral microanalyzer (JEOL, Japan) equipped with five wave (WD) and one energy-dispersive (ED) spectrometers (EPMA) at the IGEM Analytics Center for Collective Use (analyst E.V. Kovalchuk). To determine the amount of macrocomponents and main impurity elements (for both sulfides, Ni, Co, Cu, Sb; for arsenopyrite, Zn, Ag), the analysis was carried out at an accelerating

voltage of 20 kV, a Faraday cup current of 20 nA, an electron beam diameter of 1 μm, and time exposure of 20 s. The Au content in sulfides was also measured (detection limit (3σ) 45 ppm) by a precision method with increasing current strength and exposure time. The methodology of the analysis is detailed in (Kovalchuk et al., 2019).

Impurity elements in sulfides were studied by LA-ICP-MS on Agilent 7700x quadrupole mass spectrometers at the Institute of Mineralogy, Ural Branch, Russian Academy of Sciences (analyst D.A. Artemiev) and Thermo X Series 2 at the laboratory of IGEM RAS (analyst E.A. Minervina); the devices were equipped with a New Wave Research UP-213 laser ablation system. The flux density settings are 1.8–5.5 J/cm^2 for pyrite and 3.0–4.5 J/cm^2 for arsenopyrite. Each analysis was carried out as a dot or a line with a laser spot size of 30–55 μm. Using laser sampling, 15 point and 13 profile samples of pyrite and 12 point and 11 profile samples of arsenopyrite were analyzed. The survey parameters for different devices are described in detail in (Artemiev et al., 2017; Abramova, 2018). The external calibration standards USGS MASS-1 and UQAC FeS-1 were used. The internal standard (IS) for pyrite and arsenopyrite was ^{57}Fe. For the quantitative calculation, the iron content obtained by the EPMA method was used.

RESULTS

Conditions for Finding Pyrite and Arsenopyrite

The studied samples were represented by beresitized carbonaceous silty-sandstones with banded and disseminated mineralization and polymictic sandstones with disseminated arsenopyrite–pyrite mineralization (Figs. 2, 3).

The pyrite consisted of rounded grains with crystallographic outlines up to 300 μm across; rare subhedral pentagondodecahedral pyrite crystals were up to 50 μm in size. In silty-sandstones, the pyrite consisted of elongated aggregates, forming thin (1–1.5 mm) layers with rare arsenopyrite, with scattered small sulfide phenocrysts between layers (Fig. 2). The grains and, to a greater extent, pyrite aggregates were fractured and contained inclusions of rock-forming minerals. Their abundance of inclusions gave the pyrite a cribrose (small inclusions) and cellular (large inclusions) appearance.

Arsenopyrite was represented by euhedral, subhedral acicular crystals, up to 80 and, less often 100 μm in size, both isolated and in aggregates, intergrown with pyrite.

The samples were characterized by pyrite–arsenopyrite intergrown with marcasite (identified by optical microscope), while in sandstones, such intergrowths make up the bulk of the sulfide dissemination (Fig. 3).

Pyrite. According to the EPMA data (61 analytical points), the composition of pyrite (Fig. 4) deviates from stoichiometric due to arsenic impurity and varies from $Fe_{0.99}(As_{0.004}S_{1.996})_{\Sigma 2}$ to $Fe_{0.99}(As_{0.16}S_{1.84})_{\Sigma 2}$. Study in the BSE mode revealed that pyrite grains have fine oscillatory zoning with micron-sized growth zones, which becomes coarser towards the outer zones, transitioning into a uniform rim (Figs. 2c–2e). In single grains in cribrose and cellular zones of pyrite, in addition to inclusions of rock-forming minerals, bright (BSE) segregations up to 1 μm in size were found. Qualitatively (SEM-EDS), we were able to establish Pb–Sb- and Co–Ni-bearing minerals, according to the ratio of components, presumably jamesonite and cobaltite. In a crack in a pyrite aggregate, an Hg-bearing mineral segregation less than 1 μm in size was found.

The arsenic content in pyrite varies from 0.2 to 9.2 wt %, while the largest range of As contents is inherent to the mineral from marcasite-pyrite–arsenopyrite intergrowths (Figs. 3c, 3d). Of the impurity elements, Co (up to 0.07 wt %) and Cu (up to 0.15 wt %) were found. Ni and Sb are noted in single analyses at the detection limit. Table 1 shows the concentrations of impurity elements in pyrite with am occurrence frequency in samples of 90–100%, obtained by LA-ICP-MS. Ag was found above the detection limit in 82% of samples; Hg, in 76%; and Tl, in 78%. Other elements found in single samples, with a frequency of occurrence of 20–30%: Mn (up to 20 ppm), Zn (up to 650 ppm), Ga (up to 1 ppm), Sn (up to 0.9 ppm), Te (up to 2 ppm).

Two types of zoning have been established in pyrite grains from sulfide layers and disseminations. Although the diameter of the analytical laser beam averaged 5- to 10-μm zones, when comparing the EPMA and LA-ICP-MS data in pyrite grains and aggregates, three zones contrasting in the distribution of elements of the studied complex were established. The first, central (Fig. 2, under number 1), depleted in As (1.5–1.9 wt %), Co (7–30 ppm), Ni (18–100 ppm), Au (up to 5 ppm), and with elevated Sb (~65 ppm), Hg (~30 ppm), Pb (~ 30 ppm) with respect to the second bright (outer) zone (Fig. 2, under number 2) with an As content of up to 5.4 wt %, Co (50–70 ppm), Ni (350–370 ppm), Au (GM 13.5), Cu (~260 ppm), Sb (~35 ppm), Hg (3–7 ppm), Pb (~15 ppm); and the third, dark rims, with an As content of about 3 wt % (Fig. 2—under the number 3). Rims can be from thin and barely noticeable up to 40 μm thick.

Based on a few ablation points, it was established that in the dark rims along the boundaries of zones (Fig. 2d, number 3), there was a reduced content of (ppm): Co (<0.4 to 1.5), Ni (<2 to 13), Cu (24–55), Sb (2–5), Pb (0.6–10); and increased content of Au (20–30 ppm). Cribrose and cellular areas are often observed

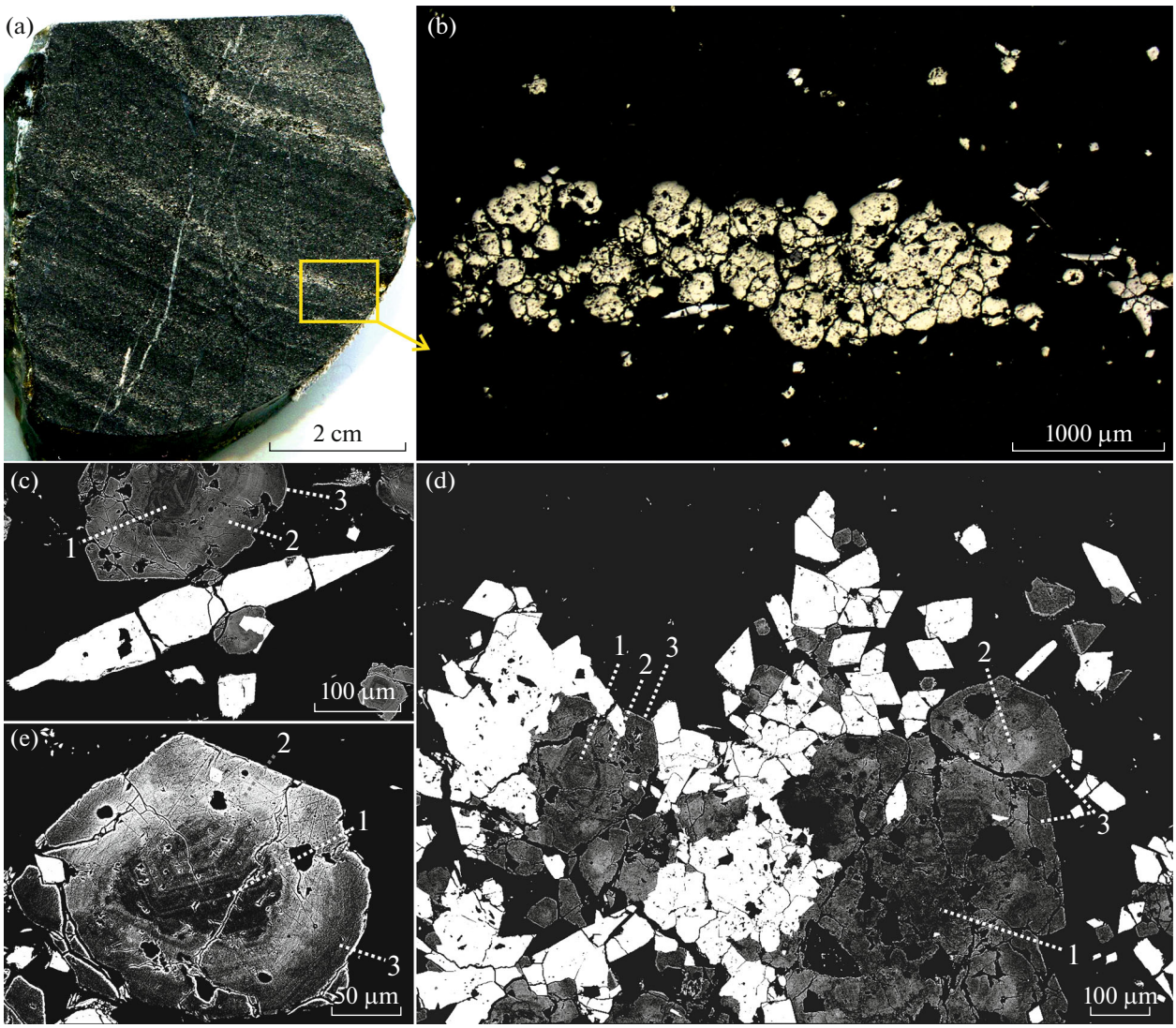

Fig. 2. Disseminated ores with pyrite-saturated layers of Kyuchus deposit. (a) macrophoto of silty-sandstones; (b) enlarged fragment of arsenopyrite–pyrite layers (photo in reflected light of optical microscope); (c–e) aggregates of intergrowths of arsenopyrite (bright phases) and zoned pyrite, BSE image, pyrite zones indicated by numbers: (1) central; (2) outer light zone; (3) rims.

along transition boundaries from the central to the outer zones and result from fine dissemination of fragments of the carbonaceous–silicate matrix. In the ablation spectra of cribrose regions of grains, elements are distributed in groups (e.g., Co, Ni, Au, Sb, Pb, Hg, etc. (Fig. 5)), which suggests the presence of microinclusions of other minerals: sulfides and native gold. A significant positive correlation in pyrite was established for the pairs Co–Ni (r = 0.95), Cu–As (r = 0.8), Ag–Sb (r = 0.84), Ag–Hg and Ag–Pb (r = 0.7), Pb–Sb (r = 0.86), and Pb–Bi (r = 0.7) for N = 33 (Fig. 6). No significant correlation of Au with the above elements was found.

In fine pyrite crystals from disseminated zones, zoning was established due to arsenic-enriched central zones and pronounced arsenic-depleted rims (Fig. 3c).

According to the EPMA data, the gold content in pyrite exceeds the detection limit in approximately half the point analyses, reaching 0.03 wt %, while the majority of spot analyses of pyrite with a gold content above the detection limit falls within the As content range of 2–5 wt % (Fig. 7b). Elevated Au concentrations are recorded in the pyrite rims of both banded and disseminated ores.

Arsenopyrite. Scanning the surface of slices of arsenopyrite grains in backscattered electrons revealed zoning with an increase in the amount of As and, accordingly, a decrease in the amount of S from the center to the edge (Figs. 8a, 8b). The composition of arsenopyrite (Fig. 4) varies within $Fe_{1.00}(As_{0.68}S_{1.21})_{\Sigma 1.89}$–$Fe_{1.00}(As_{0.90}S_{1.08})_{\Sigma 1.98}$; the As/S ratio (at %) varies from 0.56 to 0.86. Of the impurity

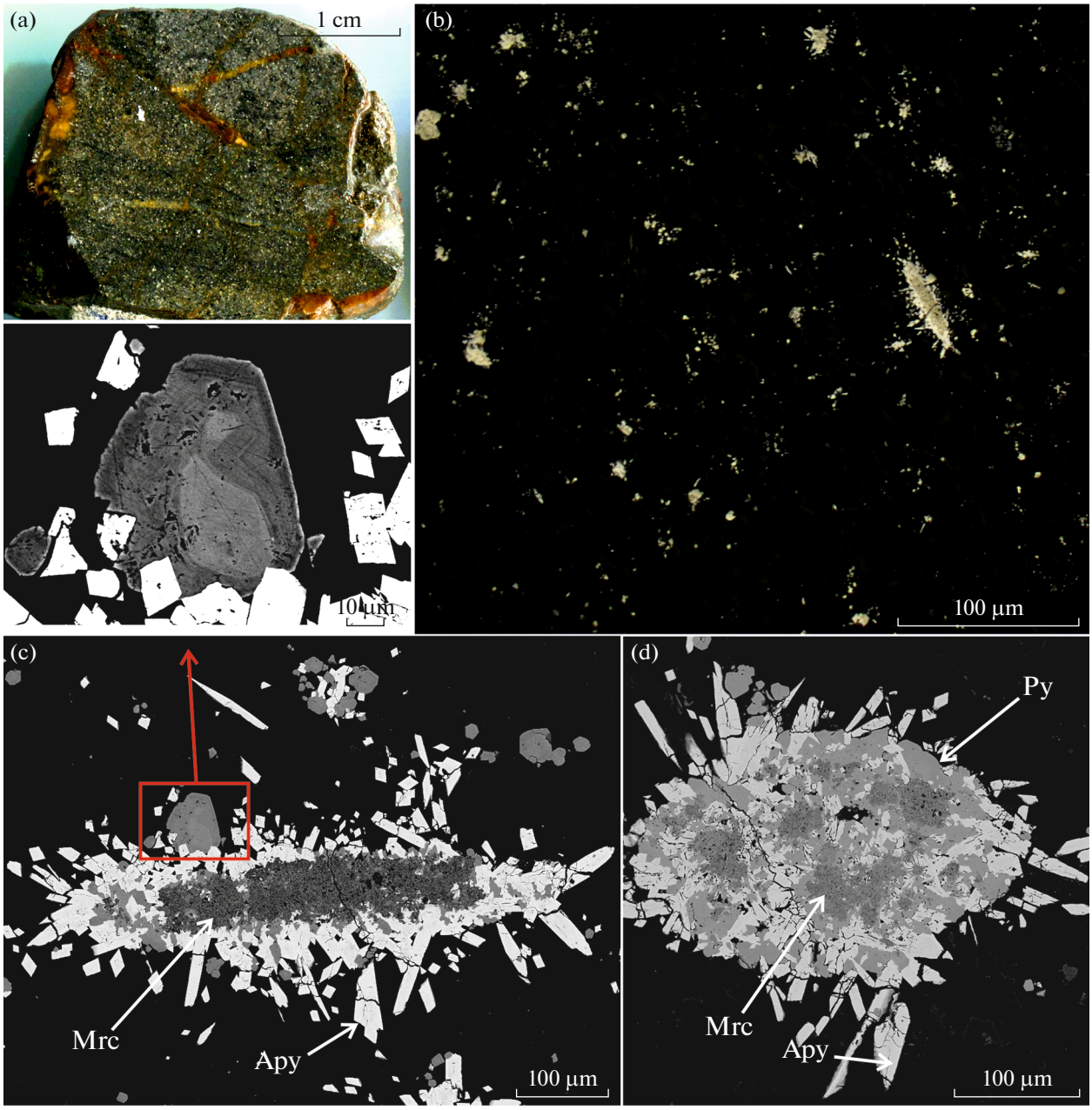

Fig. 3. Disseminated ores of Kyuchus deposit: (a) macrophoto of sandstones with enlarged fragment of disseminated sulfides (b) photo in reflected light of optical microscope); (c, d) pyrite(Py)–arsenopyrite(Apy)–marcasite(Mrc) intergrowths of disseminated ores with enlarged fragment of zoned pyrite, BSE images.

elements, the following were found: Sb—from ≥0.06 to 0.5 wt %; Co, from ≥0.06 to 0.08 wt %. Ni, Cu, and Ag are noted in isolated cases in amounts at the level of their detection limit.

According to EPMA, Au in arsenopyrite was found in 21 out of 49 analyses, reaching 0.2 wt %, while its amount increases towards the edges of crystals (similar to the behavior of As (Fig. 8)). It should be noted that such zoning of gold and arsenic contents in arsenopyrite, similar to arsenic pyrite, was revealed for the first time in ores of the Kyuchus deposit.

Based on the LA-ICP-MS results, constantly occurring impurities in arsenopyrite are Co, Ni, Sb, Au, Pb, Bi, Cu, Hg. The following regularity in the distribution of trace elements was revealed: antimony features increased concentrations in the central zones of crystals (Fig. 8b, dark zones); cobalt and nickel have a similar distribution (correction factor = 0.93 for N = 24), as an isomorphous impurity; their amount often

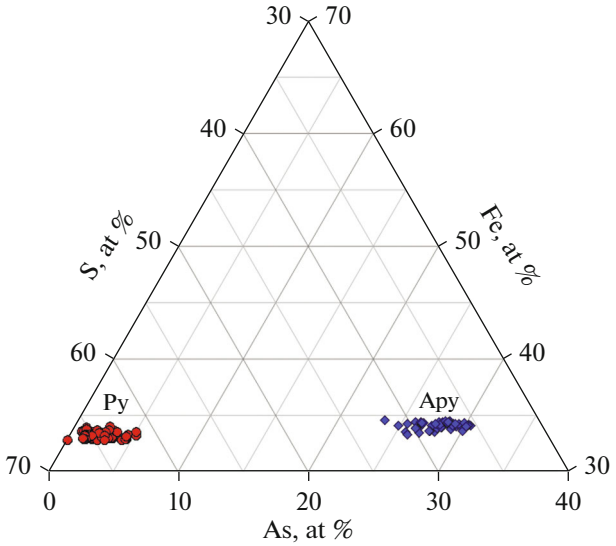

Fig. 4. Compositions of pyrite and arsenopyrite on Gibbs triangle.

increases towards the edges of the grains, and these elements, together with Cu, Ag, Bi, Pb, are part of inclusions of other sulfides; lead in amounts up to 5 ppm has a uniform distribution in the spectra, while in amounts >5 ppm, spikes together with Ag–Bi–Co–Ni; less frequently, Au, Cu, Sb; copper, bismuth, mercury, and thallium feature joint spikes in spectra with other elements (Pb–Ag–Co–Ni–Zn–Au). A positive significant correlation in arsenopyrite was established for the pairs Ag–Cu ($r = 0.8$), Ag–Hg ($r = 0.91$), and Sb–Bi ($r = 0.84$) (Fig. 5). Based on the LA-ICP-MS results, Au in arsenopyrite has no significant correlations with other elements.

The Au distribution in the ablation spectra of arsenopyrite can be divided into two types: (1) joint spikes with Hg–Cu–Ag (often together with spikes of Pb–Bi–Co–Ni–Zn–Tl signals)—here we can assume the presence of fine native gold with impurities together with galena, sphalerite, and other minerals; (2) uniform distribution in the spectra with an increase from the center to the edge of the grain. Such a distribution can be observed in single spectra with the absence of

Table 1. Main impurity elements in pyrite and arsenopyrite, according to LA-ICP-MS data

C, ppm		Co	Ni	Cu	Ag	Ge	Sb	Au	Hg	Tl	Pb	Bi
Py	Min	0.4	3.6	24	<0.08	<0.9	2	0.9	<2.3	<0.02	0.6	0.06
	Max	81	404	698	4.7	7	339	115	32	1.7	87	2.1
	GM	17	68	164	0.5	2.5	42	7.4	8.9	0.2	17	0.6
	N	94	94	100	82	94	100	100	76	79	100	97
Asp	Min	1.5	13	11.5	<0.3	<0.9	391	1.2	<11	<0.07	4.4	0.15
	Max	377	1347	188	20	5	4080	487	184	7.6	78	4.3
	GM	43	188	39	2.6	–	1147	38	46	0.9	16	0.8
	N	100	100	88	80	70	100	100	88	83	100	100

Note. For each component, minimum (min), maximum (max), and geometric mean values are indicated, calculated by formula $GM(x_1, x_2, \ldots, x_n) = \sqrt[n]{x_1 x_2 \ldots x_n}$, where x_1, x_2, ..., x_n are the average values of a component at a point, profile, or profile segment); N is occurrence frequency, %.

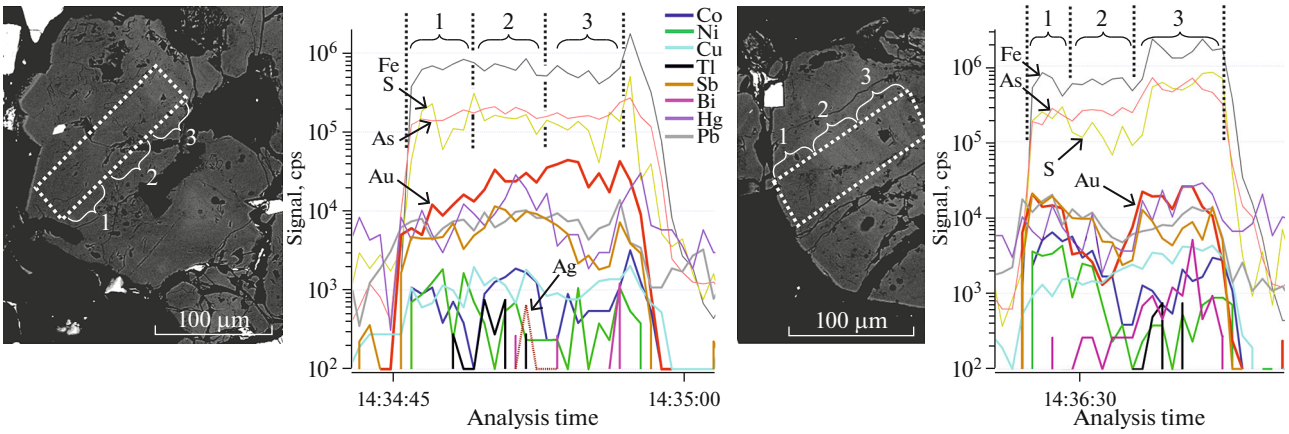

	Co	Ni	Cu	Ag	Sb	Au	Hg	Tl	Pb	Bi
min	9	66	148	–	27	32	–	–	22	0.1
max	20	153	229	2	62	102	18	0.3	31	1.3

	Co	Ni	Cu	Ag	Sb	Au	Hg	Tl	Pb	Bi
min	7	26	240	–	20	11	–	–	16	0.3
max	64	510	300	–	106	46	10	0.1	57	1.8

Fig. 5. Distribution spectra of elements according to ablation profiles (indicated by dotted lines) in pyrite; numbers indicate corresponding zones in profiles and spectra; tables show minimum and maximum contents (ppm) of elements by profiles.

Ag and Hg and with an Au–Sb inverse correlation and a direct Au–As correlation. In this case, the outer rims of arsenopyrite are enriched in gold (Fig. 8c).

DISCUSSION AND CONCLUSIONS

For the pyrite–arsenopyrite assemblage of disseminated ores at the Kyuchus deposit, the range of concentrations and nature of the distribution of "invisible gold and trace elements in sulfides have been established. Arsenopyrite is characterized by elevated contents of Ni and Co, Sb, Au, Hg, and Ag compared to pyrite. Such a distribution of elements can be associated with a change in the composition of the solution and crystallization conditions, as well as with the growth kinetics of fine-prismatic arsenopyrite. The copper concentration is higher in arsenic pyrite, while Pb, Bi, and Tl have approximately the same contents for both sulfides. Elevated concentrations of gold in arsenopyrite with respect to pyrite have been noted for many deposits and are consistent with empirical data, indicating the equilibrium of coexisting pyrite and arsenopyrite (Mumin et al., 1994; Fleet and Mumin, 1997; Morey et al., 2008; Sung et al., 2009; Cook et al. 2003).

In pyrite, the maximum concentrations of Co, Ni, Cu, Hg, Pb, Sb, Au, Bi, as well as less common Zn, Te, Mn, Tl, Ge, Ga, are found in porous, cribrose regions of grains or at the boundaries of zones and microcracks. In arsenopyrite, the distribution of elements is similar, with the exception of Sb (maximum antimony concentrations in the center of grains, pronounced zoning), and Au (maximum gold concentrations are clearly confined to thin outer rims). Joint spikes of signals of other elements in porous cribrose areas of pyrite and arsenopyrite may be the result of trapping of material from the carbonaceous–silicate rock matrix.

The absence of a significant correlation between Au and other elements in both pyrite and arsenopyrite suggests that some gold was concentrated in sulfides during their growth, mainly in acicular arsenopyrite. Another part of gold, together with a group of elements (As–Sb–Tl–Hg–Pb–Bi–Ag–Cu–Zn, etc.), is present in fragments of the carbonaceous–silicate matrix in cellular and cribrose zones of pyrite and arsenopyrite. This is what caused the spike in all the indicated elements in the ablation spectrum (Fig. 5, right spectrum).

Enrichment in gold and arsenic of the edge parts of pyrite and arsenopyrite crystals has been established. Earlier, such zoning was observed in crystals and intergrowths of auriferous pyrite and marcasite (Wilson et al., 2002; Volkov and Sidorov, 2016; Novozhilov and Gavrilov, 1999; Cline, 2001). Judging from the relationships of sulfides, arsenopyrite crystallized later than pyrite and the revealed zoning may indicate the development of arsenopyrite after aggregates of earlier gold-bearing As-pyrite. Moreover, the As content in pyrite varies from 0.2 to 9 wt %, which is comparable to the amount of arsenic in pyrite from Carlin-type gold deposits, while the distribution of impurity elements is different. In pyrite from Carlin-type deposits, the outer rims are enriched in gold, together with other elements, which grow on pyrite depleted in impurities (Muntean et al., 2011; Large et al., 2009; Large and Maslennikov, 2020). In pyrite metacrystals of the Kyuchus deposit, the outer zones, as well as rims, are

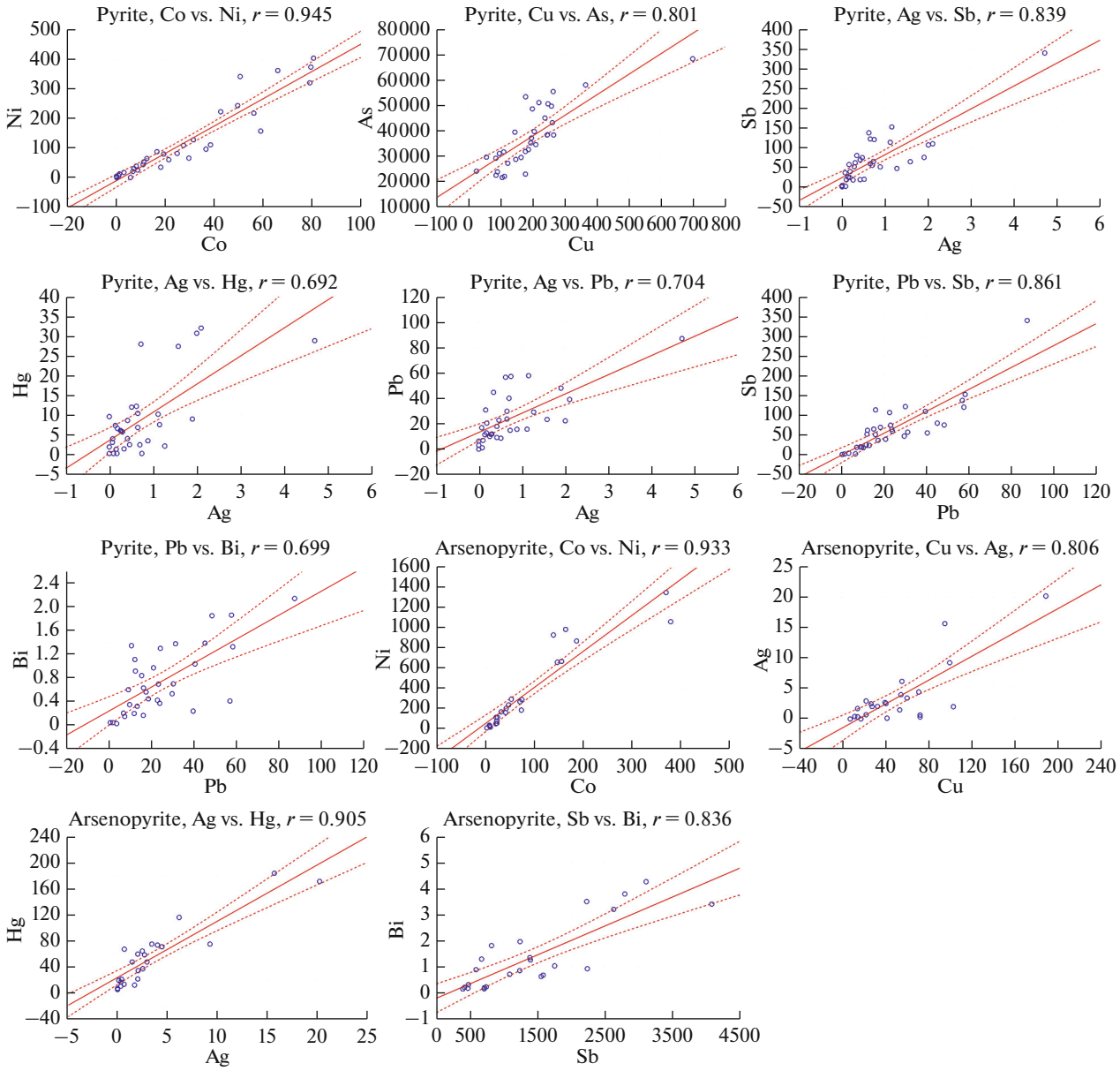

Fig. 6. Diagrams of pair correlations of elements in pyrite and arsenopyrite; *r*, correlation coefficient; dotted lines, confidence interval (95%).

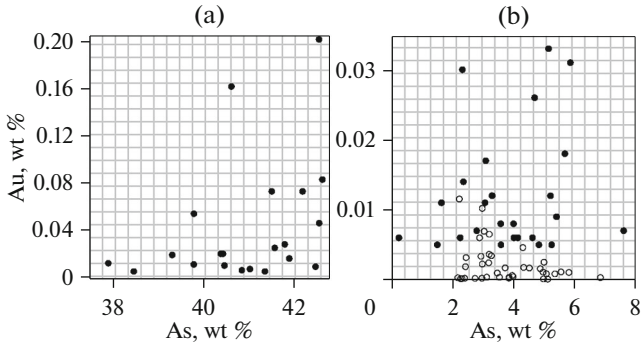

Fig. 7. Diagram of Au and As contents (in wt %) in arsenopyrite (a) (based on EPMA results) and pyrite (b) (EPMA and LA-ICP-MS, empty circle) of Kyuchus deposit.

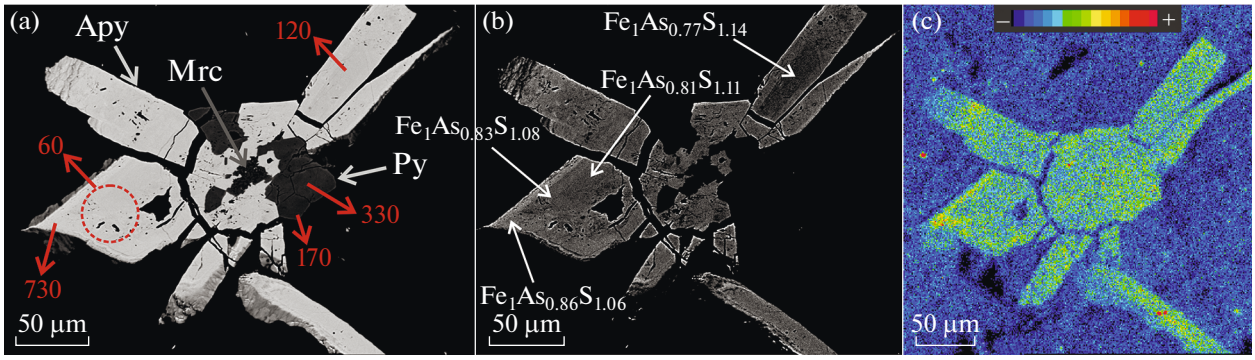

Fig. 8. Intergrowth of acicular arsenopyrite (Apy), pyrite (Py), and marcasite (Mrc): (a, b) image in backscattered electrons, numbers indicate amount of Au (in ppm) obtained by EPMA and LA-ICP-MS (dotted line indicates ablation diameter); (b) image with increased contrast—amount of As increases from center to edge in arsenopyrite; (c) Au distribution map, shooting conditions: Au (Mα, PETH), current 20 nA, time at point 60 ms.

enriched in gold, as well as other elements, which, in turn, are depleted in other elements. This element distribution could have resulted from recrystallization of diagenetic sulfides (pyrite and marcasite) and further growth of faceted rims of newly formed pyrite.

The results indicate the possible formation of orebodies at deposits due to two sources: remobilization of ore components from host carbonaceous terrigenous rocks and inflow of fluids rich in gold.

ACKNOWLEDGMENTS

The authors are grateful to S.G. Kryazhev for samples provided for research, as well as to N.S. Bortnikov and V.A. Sidorov for criticism and valuable recommendations.

FUNDING

The research was carried out with the financial support of the basic theme of IGEM RAS and the Russian Foundation for Basic Research (project 18-05-70001 “Arctic Resources”).

CONFLICT OF INTEREST

The author declares that he has no conflict of interest.

REFERENCES

Abramova, V.D., Inductively coupled plasma mass-spectrometry with laser sampler in study of PGE distribution in the magmatic sulfides, *Metallogeniya drevnikh i sovremennykh okeanov* (Metallogeny of Ancient and Modern Oceans), 2018, no. 1, pp. 256–258.

Artem’ev, D.A., Maslennikov, V.V., and Filippova, K.A., Inductively coupled plasma and laser ablation mass-spectrometry in the minerlogical–geochemical studies of the Institute of Mineralogy of UrO RAN, *Metallogeniya drevnikh i sovremennykh okeanov* (Metallogeny of Ancient and Modern Oceans), 2017, no. 1, pp. 201–206.

Berzon, R.O., Bryzgalov, I.A., Konyshev, V.O., Meshcherina, T.V., and Nekrasova, A.N., Geological setting, mineral composition, and formation conditions of the Kyuchus gold–mercury deposit (Sakha, Russia), *Geol. Ore Deposits,* 1999, vol. 41, no. 6, pp. 440–459.

Bortnikov, N.S., Gamyanin, G.N., Vikent’eva, O.V., Prokof’ev, V.Yu., and Prokopiev, A.V., The Sarylakh and Sentachan gold–antimony deposits, Sakha-Yakutia: a case of combined mesothermal gold–quartz and epithermal stibnite ores, *Geol. Ore Deposits,* 2010, vol. 52, no. 5, pp. 339–372.

Cabri, L.J., Chryssoulis, S.L., De Villiers, J.P.R., Laflamme, J.H.G., and Buseck, P.R., The nature of “invisible” gold in arsenopyrite, *Can. Mineral.,* 1989, vol. 27, pp. 3–362.

Cabri, L.J., Newville, M., Gordon, R.A., Crozier, E.D., Sutton, S.R., McMahon, G., and Jiang, D.-T., Chemical speciation of gold in arsenopyrite, *Can. Mineral.,* 2000, vol. 38, pp. 1265–1281.

Cathelineau, M., Boiron, M.C., Holliger, P., Marion, P., and Denis, M., Gold in arsenopyrites: crystal chemistry, location and state, physical and chemical conditions of deposition, *Econ. Geol. Monogr.,* 1989, vol. 6, pp. 328–341.

Chryssoulis, S.L. and Cabri, L.J., The significance of gold mineralogical balances in mineral processing, *Instit. Mining Metallurgy Trans.,* 1990, vol. 99, C1–C9.

Cline, J.S., Timing of gold and arsenic sulfide mineral deposition at the Getchell Carlin-type gold deposit, north-central Nevada, *Econ. Geol.,* 2001, vol. 96, pp. 75–89.

Cook, N.J., Ciobanu, C.L., Meria, D., Silcock, D., and Wade, B., Arsenopyrite-pyrite association in an orogenic gold ore: tracing mineralization history from textures and trace elements, *Econ. Geol.,* 2013, vol. 108, pp. 1273–1283.

Fleet, M.E. and Mumin, A.H., Gold-bearing arsenian pyrite and marcasite and arsenopyrite from Carlin trend gold deposits and laboratory synthesis, *Am. Mineral.,* 1997, vol. 82, pp. 182–193.

Genkin, A.D., Lopatin, V.A., Savel’ev, R.A., Safonov, Yu.G., Sergeev, N.B., Kerzin, A.L., Tsepin, A.I., Amshtutts, Kh., Afanas’eva, Z.B., Vagner, F., and Ivanova, G.F., Gold ores of the Olimpiada deposit (Yenisei Ridge, Siberia), *Geol. Rudn. Mestorozhd.,* 1994, vol. 36, no. 2, pp. 111-136.

Genkin, A.D., Bortnikov, N.S., Cabri, L.J., Wagner, F.E., Stanley, C.J., Safonov, Y.G., McMahon, G., Friedl, J., Kerzin, A.L., and Gamyanin, G.N., A multidisciplinany study of invisible gold in arsenopyrite from four mesothermal gold deposits in Siberia, Russian Federation, *Econ. Geol.,* 1998, vol. 93, pp. 463–487.

Konyshev, V.O., Model of gold ore field in structures of the tectonomagmatic activation, Kyuchyus deposit, *Rudy Met.,* 1995, no. 4, pp. 52–64.

Kovalchuk, E.V., Tagirov, B.R., Vikentyev, I.V., Chareev, D.A., Tyukova, E.E., Nikol'sky, M.S., Borisovsky, S.E., and Bortnikov, N.S., "Invisible" gold in synthetic and natural arsenopyrite crystals, Vorontsovka Deposit, Northern Urals, *Geol. Ore Deposits,* 2019, vol. 461, no. 5, pp. 447–468.

Kovalev, K.R., Kalinin, Yu.A., Polynov, V.I., Kydyrbekov, E.L., Borisenko, A.S., Naumov, E.A., Netesov, M.I., Klimenko, A.G., and Kolesnikova, M.K., The Suzdal gold–sulfide deposit in the black shale of Eastern Kazakhstan, *Geol. Ore Deposits,* 2012, vol. 54, no. 4, pp. 254–275.

Large, R.R., Danyushevsky, L., Hollit, C., Maslennikov, V., Meffre, S., Gilbert, S., Bull, S., Scott, R., Emsbo, P., Thomas, H., Singh, B., and Foster, J., Gold and trace element zonation in pyrite using a laser imaging technique: implications for the timing of gold in orogenic and Carlin-style sediment-hosted deposits, *Econ. Geol.,* 2009, vol. 104, pp. 635–668.

Large, R.R. and Maslennikov, V.V., Invisible gold paragenesis and geochemistry in pyrite from orogenic and sediment-hosted gold deposits, *Minerals,* 2020, vol. 10, no. 4, p. 339.

Morey, A.A., Tomkins, A.G., Bierlein, F.G., Weinberg, R.F., and Davidson, G.J., Bimodal distribution of gold in pyrite and arsenopyrite: examples from the Archean Boorara and Bardoc shear zones, Yilgarn Craton, Qestern Australia, *Econ. Geol.,* 2008, vol. 103, pp. 599–614.

Moskvitina, L.V., Moskvitin, S.G., and Anisimova, G.S., Research of nanoscale gold by methods of tunneling and atomic-powered microscopy with chemical and ion-plasma etching in the Kuchus deposit (Republic Sakha (Yakutia), *IOP Conf. Series: Earth and Environmental Science,* 2019, p. 022184.

Mumin, A.H., Fleet, M.E., and Chryssoulis, S.L., Gold mineralization in As-rich mesothermal gold ores of the Bogosu–Prestea mining district of the Ashanti gold belt, Ghana: remobilization of "invisible" gold, *Mineral. Deposita,* 1994, vol. 29, pp. 445–460.

Muntean, J.L., Cline, J.S., Simon, A.C., and Longo, A.A., Magmatic-hydrothermal origin of Nevada`s Carlin-type gold deposit, *Nature Geosci.,* 2011, no. 4, pp. 122–127.

Novozhilov, Yu.I. and Gavrilov, A.M., *Zoloto-sul'fidnye mestorozhdeniya v terrigennykh uglerodistykh tolshchakh* (Gold–Sulfide Deposits in Terrigenous Carbonaceous Sequences), Moscow: TsNIGRI, 1999.

Ridley, W.I. and Koenig, A.E., Development of sulfide calibration standards for the laser ablation inductively-coupled plasma mass spectrometry technique us government, *J. Analyt. At. Spectrom.,* 2002, vol. 17, pp. 406–409.

Sung, Y.H., Brugger, J., Ciobanu, C.L., Pring, A., Skinner, W., and Nugus, M., Invisible gold in arsenian pyrite and arsenopyrite from a multistage Archaean gold deposit: Sunrise Dam, Eastern Goldfields Province, Western Australia, *Mineral. Deposita,* 2009, vol. 44, p. 765.

Volkov, A.V. and Sidorov, A.A., Geological-genetic model of the Carlin-type gold deposits, *Litosfera,* 2016, no. 6, pp. 145–165.

Volkov, A.V. and Sidorov, A.A., Invisible gold, *Vestn. RAN,* 2017, vol. 87, no. 1, pp. 40–49.

Volkov, A.V., Genkin, A.D., and Goncharov, V.I., Gold speciation in ores of the Natalka and Maiskoe deposit (Nortehast Russia), *Tikhookean. Geol.,* 2007, vol. 25, no. 6, pp. 18–29.